Available online at www.sciencedirect.com

jmr&t Journal of Materials Research and Technology

www.jmrt.com.br

Original Article

A comparative study of electrochemical corrosion behavior in Laser and TIG welded Ti–5Al–2.5Sn alloy

Muhammad Shamir[a], *Massab Junaid*[b,*], *Fahd Nawaz Khan*[c], *Aqeel Ahmad Taimoor*[d], *Mirza Nadeem Baig*[e]

[a] *School of Chemical and Materials Engineering, National University of Sciences and Technology, Islamabad, Pakistan*
[b] *Faculty of Mechanical Engineering, GIK Institute of Engineering Sciences and Technology, Topi, Pakistan*
[c] *Faculty of Materials and Chemical Engineering, GIK Institute of Engineering Sciences and Technology, Topi, Pakistan*
[d] *Department of Chemical and Materials Engineering, Faculty of Engineering, King Abdul Aziz University, Jeddah, Saudi Arabia*
[e] *Pakistan Welding Institute, PO Box 1781, Islamabad, Pakistan*

ARTICLE INFO

Article history:
Received 2 May 2017
Accepted 8 September 2017
Available online 20 November 2017

Keywords:
Galvanic corrosion
EIS
Laser welding
TIG welding
Ti–5Al–2.5Sn

ABSTRACT

Corrosion behavior of TIG and laser welded Ti–5Al–2.5Sn alloy was compared using different electrochemical techniques. Bead on plate (BoP) configuration was used for welding of 1.6 mm thick Ti–5Al–2.5Sn plates which led to the formation of complete α′ martensitic structure in laser welds and acicular α along with α′ martensite within coarse prior β grains was observed in TIG welds. Potentiodynamic and cyclic polarization were carried out in 5, 7 and 9 M HNO_3 to study the effect of concentration on the galvanic corrosion of laser and TIG welded Ti–5Al–2.5Sn. The oxide layer developed after 192 h of immersion in fuming HNO_3 was studied using electrochemical impedance spectroscopy (EIS) and SEM. All the samples showed good passivity but different oxidation behavior was observed mainly because of the surface modification after the welding operation.

1. Introduction

Titanium alloys are extensively used in high performance structural applications in addition to biomedical applications [1]. Most of the applications of titanium alloys include aerospace, automotive, petrochemical plants, power generation and marine structures, owing to their excellent strength to weight ratio, creep properties, and resistance to corrosion [2–4]. In all the above applications titanium alloys have to undergo certain manufacturing operations, including machining, joining, cutting, etc. With increased applications of titanium alloys in the various industries, welding methods like friction welding, electron beam welding (EBW), laser beam welding (LBW), laser hybrid welding, TIG welding have

* *Corresponding author.*
E-mail: massab@giki.edu.pk (M. Junaid).

https://doi.org/10.1016/j.jmrt.2017.09.006

Nomenclature

EIS	electrochemical impedance spectroscopy
FZ	fusion zone
HAZ	heat affected zone
HCP	hexagonal closed pack
Cp Ti	commercially pure titanium
OM	optical microscopy
SEM	scanning electron microscopy
XRD	X-ray diffraction
BoP	bead on plate
α	alpha phase
α′	alpha martensite
β	beta phase

been developed and are widely used for the joining of titanium alloys for different applications [5–11].

Titanium undergoes a phase transformation from HCP (alpha phase), to BCC (beta phase) and this transformation temperature is referred to as beta transus temperature. Beta transus temperature varies for different titanium alloys and is due to the different alloying addition or impurities present in the alloy [12]. Titanium alloys are characterized as commercially pure (CP) titanium, alpha titanium alloys, alpha–beta titanium alloys and beta titanium alloys. Alpha alloys or near alpha alloys exhibit better creep properties and strength at high temperatures than alpha–beta and beta alloys [13]. Among the alpha titanium alloys, those containing aluminum, tin and/or zirconium are preferred for high temperature applications [14]. One of the benefits of the alpha titanium alloys is their good weldability as the joint properties are superior to the Base Metal (BM). This is owing to the formation of α′ martensite and acicular α, which have higher hardness than the BM [15]. However, the presence of β stabilizers in β titanium alloys suppresses the formation of α′ martensite, resulting in strength of weld joint to be less than the BM. Ti–5Al–2.5Sn is an α titanium alloy which is mostly used in the aerospace application requiring high temperature strength [14,16]. Furthermore, it has low cost alloying elements as compared to the well-known Ti–6Al–4V, which is considered to be the 'work horse' of aerospace industry [14].

Titanium has a strong affinity for oxygen and the resultant surface oxide layer is very protective, highly adherent and stable and the excellent corrosion resistance of titanium alloys is attributed to this protective oxide layer. The corrosion resistance of titanium alloys is affected when this oxide layer does not remain completely adherent and breaks, thereby exposing the underneath surface. Reducing agents and very powerful oxidizing environments compromise the protective nature of the oxide layer, thereby degrading it [17,18]. The work of Lu et al. [7], and Barreda et al. [19] showed that the high affinity of titanium to react with atmospheric gases such as oxygen and nitrogen at temperatures above 350 °C makes it challenging to produce good quality weldments [7,19]. The reaction with atmospheric gases leads to the contamination of the molten pool and induces embrittlement in the weldment, resulting in reduced ductility and toughness. Therefore, to protect the molten pool from gaseous contamination, application of shielding gas during the welding operation is mandatory in conventional arc and laser welding process. The mechanical properties of weldments are significantly influenced by the fusion zone (FZ) oxidation, hence this phenomenon is very important to study [20]. A review of literature showed that the color of weld bead is considered as an indication of FZ oxidation. For instance, for TIG welding of Cp Ti, bright silvery appearance of the weld bead showed minimal contamination and adequate shielding as opposed to blue, purple and gray appearance [9]. Similarly Li et al. reported that a blue colored bead appearance in laser welding of Cp Ti contains highest oxygen contents while silver color showed lowest concentration of oxides [21]. Although the weld bead color indicates the level of contamination due to poor shielding of the weld pool [22], however, EDX analysis will provide a better estimate of FZ oxidation [23].

Both conventional and solid state welding techniques are employed for joining of titanium alloys [24]. However, conventional arc welding is mostly used due to ease of automation and low cost operation [25]. Furthermore, laser welding has also proven to be very effective especially for titanium alloys due to its focused and dense heat source and low heat input resulting in narrow heat affected zone [11]. Laser welding has certain key beneficial aspects compared to the conventional arc welding process and therefore is being used as an alternative welding process. Short, 2009 reported that the power density for laser welding is in the range of approx. 10^{12} W/m^2, whereas, it is approx. 10^9 W/m^2 for the conventional TIG welding process [25]. This high power density for laser welding results in high penetration in a single pass resulting in a reduced overall heat input. Therefore, the grains in the weld zone are relatively fine, hence narrower HAZ and reduced structural distortions are observed as compared to TIG welding process.

Weldments of alpha titanium alloys exhibit corrosion resistance similar to that of the BM and these titanium alloys containing very little alloying elements, do not respond to different heat treatments. Alpha type CP titanium weldments generally do not experience corrosion limitation in welded components. However, under active or marginal conditions, for which corrosion rates exceeding 100 μm/year, weldments may undergo accelerated corrosion. The factor identified for this accelerated corrosion rate is the transformed beta phase after welding, which is present in fusion zone and associated heat affected zone (HAZ) [17]. Alpha titanium alloys weldments are prone to stress corrosion cracking (SCC), which primarily depends on the composition of the alloy. Presence of aluminum increases the susceptibility of SCC due to the formation of an intermetallic phase Ti_3Al also known as alpha-2 in the fusion zone. As the amount of Ti_3Al increases in the microstructure, the susceptibility of SCC of the titanium alloy increases [26,27].

There are a number of environments in which alpha titanium alloy is susceptible to SCC which includes nitric acid [28]. For such applications, the conventional low carbon austenitic stainless steel is unacceptable and alpha titanium alloys are preferred over stainless steels as they possess outstanding corrosion properties. Ti–5Al–2.5Sn is an alpha alloy, which can be used for such applications and has an advantage of being readily welded. In the present work, the weldability of

Table 1 – Composition of Ti–5Al–2.5Sn. (wt. %) and mechanical properties.

Alloy composition			Tensile strength, MPa	Yield strength, MPa	Elongation, %
Ti	Al	Sn			
Bal.	5	2.5	861.8	806.6	16

Ti–5Al–2.5Sn is examined and the effect of welding techniques on the corrosion properties is monitored.

2. Experimental materials and methods

2.1. *Welding of Ti–5Al–2.5Sn*

In the present work, butt welding was carried out on the Ti–5Al–2.5Sn alloy in the mill annealed condition and Table 1 shows the chemical composition and mechanical properties of Ti–5Al–2.5Sn alloy. Full penetration bead-on-plate welds were performed using Sintec 600W Pulsed Nd:YAG and TIG arc on Ti–5Al–2.5Sn plate with dimension of 100 mm × 80 mm × 1.6 mm, as shown in Fig. 1. The welding performed was autogenous with no filler material being used. Laser welding was performed using a current of 260 A, welding speed of 160 mm/min, frequency of 8 pulses/s and stand of distance of 4 mm. For TIG welding, welding speed of 32.5 mm/min, voltage of 10 V, primary current of 32 A and background current of 16 A was used. After welding, the plates were mechanically brushed, acid pickled with HF and were cleaned with acetone. As titanium is very reactive to atmospheric gases at high temperatures, argon was used as shielding gas in both the welding processes. After the welding was performed, the plates were visually inspected to observe any welding defects.

2.2. *Microstructure and phase analysis*

Samples for microstructure and phase analysis from BM and fusion zone of TIG and laser weldments were wire cut using electric discharge machining (EDM). Metallographic samples were ground mechanically using SiC paper (120, 320, 500, 1200, 4000) and polished with 1 μm Struers diamond paste suspension. The samples were etched using Kroll agent (92 ml distilled water 6 ml HNO_3 and 2 ml HF) and then with 0.2% HF. The microstructure was then observed using an Olympus optical microscope with a polarized lens. Mira 3 Tescan PC controlled scanning electron microscope (SEM), at a vacuum of 10^{-6} Pa was used for higher magnification analysis of oxide layer and also for EDX analysis. The phases present in the FZ of laser and TIG welded samples were identified using STOE X-ray diffraction machine with theta/theta diffractometer. The source used was Cu Kα, with a wavelength of 1.54 Å. The diffraction profiles were taken from 20° to 80° with a step size of 0.02° and scan time of 1 s/step.

2.3. *Electrochemical measurements*

Electrochemical corrosions tests were conducted using Gamry potentiostat PCI-4G750. The samples were removed from the welded plates using EDM and were ground using SiC paper (120, 320, 500, 1200, 4000) and polished with 1 μm Struers diamond paste suspension. These samples were then mounted using polymer resin and only the surface to be studied was exposed. The experimental setup consists of a three electrode cell containing Ag/AgCl reference electrode, a working electrode and a counter electrode. Working electrodes consists of BM, weld fusion zone of laser and TIG of Ti–5Al–2.5Sn, respectively, and were separately studied. The potentiodynamic and cyclic polarization was conducted in 5 M, 7 M and 9 M HNO_3. The other corrosive media in which different titanium alloys can be tested are Ringer's solution (for bio-medical implants application [1]) and 3.5% NaCl solution (for marine applications) [29]. Since HNO_3 provides the most severe oxidizing environment, hence in order to study the oxidation behavior of Ti–5Al–2.5Sn alloy, different concentrations of HNO_3 were used. For all the electrochemical experiments, the measurements have been repeated a minimum of three times. Tafel plots were obtained using Gamry Echem analyst software and the results were compared. The open circuit potential was also recorded for each of these samples for 60 min. For the poten-

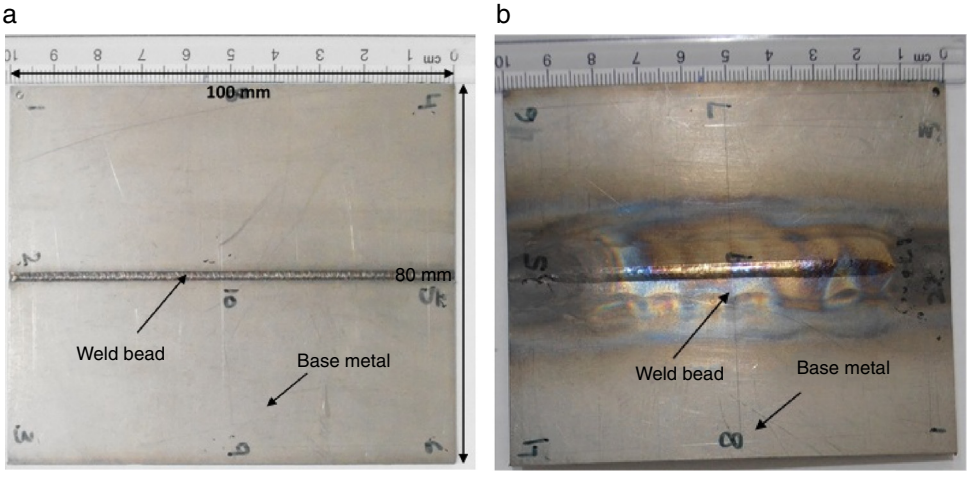

Fig. 1 – Ti–5Al–2.5Sn plates: (a) laser welded and (b) TIG welded.

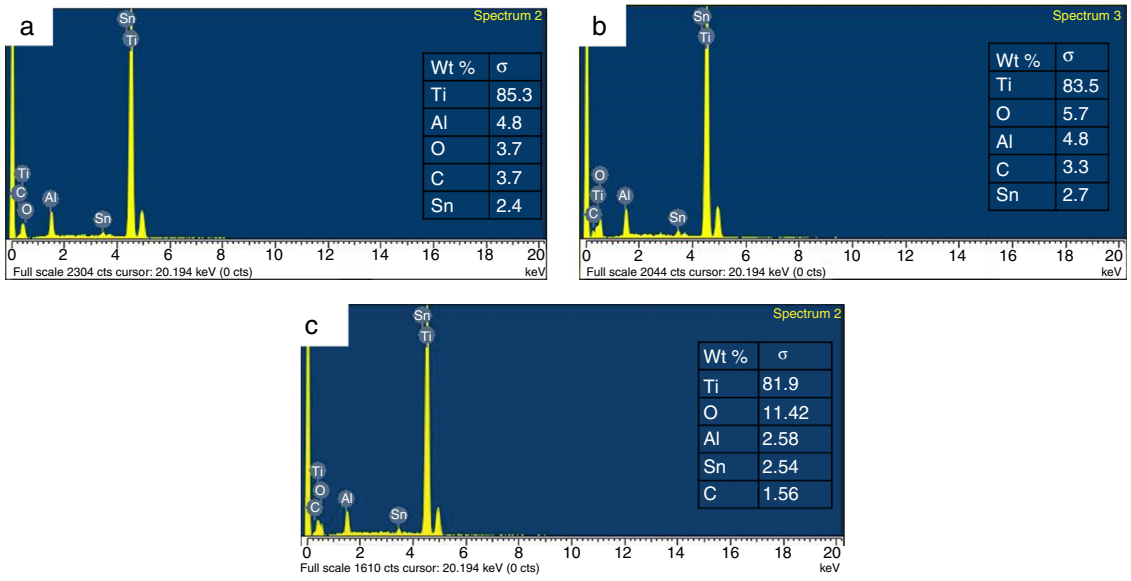

Fig. 2 – EDX analysis of: (a) BM sample, (b) FZ of laser weldment and (c) FZ of P-TIG weldment.

tiodynamic and cyclic polarization tests, the samples were held in electrolyte for 45 min before the tests. The scans were taken between −0.1 V vs. Ag/AgCl to 1.5 V vs. Ag/AgCl with a forward and reverse scan rate of 2 mV/s.

2.4. *Electrochemical impedance spectroscopy (EIS) measurements*

Electrochemical impedance spectroscopy (EIS) has been used to investigate coatings, ions transport behaviors and characteristics, due to its ability to measure high impedance system and to provide abundant electrochemical information [30–32]. Electrochemical impedance spectroscopy (EIS) was applied to determine electrochemical properties of the passive Ti–5Al–2.5Sn alloy on the welded joints. EIS spectra were recorded for the alloy/oxide electrodes after immersion in the 14.33 M HNO_3 solution. The EIS was conducted on the laser, TIG welded and BM samples. According to standard ASTM G31-12a [33], the minimum time calculated for the immersion test is approximately 140 h. However, an immersion time 192 h was reported for EIS study on Ti–6Al–4V biomedical implants [34]. Hence, after immersion in fuming HNO_3, for 192 h, EIS was performed on all the samples. According to the standard for this measurement, a sinusoidal signal of 10 mV (rms) was applied to the samples and a frequency range of 0.01 Hz to 100 kHz was used. NOVA software provided by AUTOLAB was used to evaluate the equivalent circuit of the acquired data.

3. Results and discussion

3.1. *Microstructure and phase analysis*

It appears that the weld bead is free from contamination and is of bright silvery appearance for all the two weldments as shown in Fig. 1. EDX tests were also performed on the BM sample, FZ of laser and TIG weldments and the oxygen

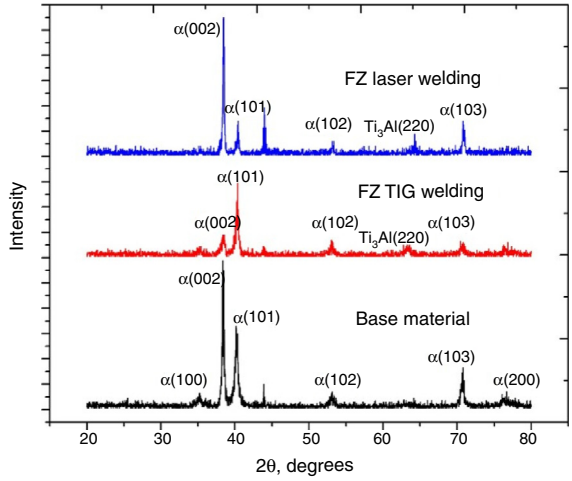

Fig. 3 – XRD patterns of BM, FZ of laser and TIG welding.

contents are reported in Fig. 2, also confirming the presence of Al and Sn as alloying elements. Among the weldments, oxygen concentration was found to be lowest in the FZ of LBW which exhibited an increase of approximately 10% compared to BM sample. The maximum oxygen contents were found in the FZ of TIG weldments which were 3 times higher than the oxygen contents of the BM sample. The reduced oxygen contents in the laser welding sample were due to the low overall heat input in the joining process. According to Baruah and Bag [35], oxygen contents of approximately 11% are considered in the acceptable range. Fig. 3 shows the XRD- spectra of the Ti–5Al–2.5Sn weldment and the phases identified are HCP α martensitic α′ and Ti_3Al. The presence of Al and Sn promotes the formation of Ti_3Al α2 phase and owing to the presence of this phase, Ti–5Al–2.5Sn is more susceptible to stress corrosion cracking. The main peaks of all the spectrums corresponded to HCP pattern which can be attributed to the presence of either α, acicular α or martensitic α′ as they have

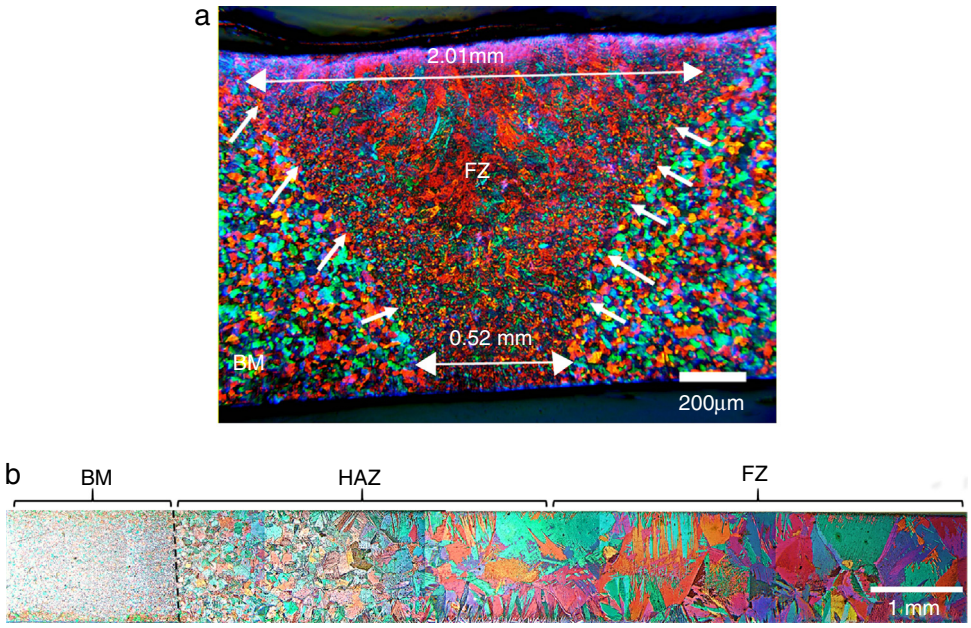

Fig. 4 – Cross-section of weld pool for (a) laser and (b) TIG weldment.

Table 2 – Width of FZ and HAZ of laser and TIG weldments.

	FZ width (mm)		HAZ width (mm)
	Top	Bottom	
TIG	6.7	4.03	7.65
Laser welding	2.01	0.52	0.75

similar crystalline structure. No sign of peaks corresponding to the bcc β phase was observed as the alloy under study is an all alpha alloy. However, in some studies on α titanium alloys, a very weak peak of residual β phase has been reported, which was attributed to low oxygen contents [36].

From the EDX analysis, it was observed that for the Ti–5Al–2.5Sn alloy under investigation, oxygen contents were found to be higher in the BM (3.7 wt%) and FZ of the TIG (11.1 wt%) and LBW (5.7 wt%). This significantly high amount of oxygen acts as an α stabilizer and suppresses the formation of β phase [36]. Fig. 4 shows low magnification macrograph of the laser and TIG welded joint in which three different zones (FZ, HAZ, and BM) based on the grain size can be observed. Furthermore the FZ/HAZ interface and HAZ/BM interface can also be seen. As compared to TIG weldments, the HAZ is a narrow region between FZ and BM for laser welding processes [10,11,37]. However, due to a much wide heat source, P-TIG welding leads to a much wider portion of a transition zone between the FZ and BM in which significant temperature rise changed the grain microstructure. Table 2 presents the width of FZ and HAZ in TIG and laser weldments. Owing to the dense nature of heat source of laser welding, the top and bottom width of FZ was significantly less than that of TIG weldments.

The optical images of the BM and FZ of TIG and laser welded samples are shown in Fig. 5, which provides an insight into the distribution of acicular α and α′ martensite in the welded samples. It can be observed in Fig. 5(a) that the BM is of equiaxed α in a prior β matrix. Furthermore, Fig. 5(b) shows that the prior β grain size increased significantly in FZ of TIG weldments, with columnar or acicular α within the grain boundaries. Similar microstructure has been reported by Karpagaraj et al. and Gao et al. for TIG welding of CpTi and Ti–6Al–4V alloys, respectively [11,22]. In Fig. 5(c), a complete α′ martensitic transformation can be seen in the FZ of laser weldments. This needle like structure resulted due to diffusion less transformation of β phase during fast cooling with a rate more than 410 °C/s [38]. Such a high cooling rate is expected in laser welding due to much focused heat input and very less over all heat input [11]. On the contrary, TIG weldments exhibited a lower cooling rate due to much higher heat input as compared to laser welding and due to this reason, complete martensitic transformation was not achieved in FZ of TIG weldments. The extent of martensitic transformation gives an estimate of the microhardness of the FZ since α′martensite is much harder than acicular α and equiaxed α phase. Due to higher proportion of martensite, the measured values of microhardness in the FZ of laser weldments was on average 26 HV more than that of TIG weldments [39,40].

3.2. *Electrochemical measurements*

The potentiodynamic polarization curves for BM, TIG welded (TIG) and laser welded (LBW) Ti–5Al–2.5Sn were obtained for different concentration of 5, 7 and 9 M HNO_3. The E_{corr} and I_{pass} values of these samples at different concentration were calculated and are presented in Table 3. Fig. 6 shows the Tafel plots of BM, TIG and laser welding at different concentrations of nitric acid. For all the samples, corrosion potential increases when acid concentration is increased from 5 M to 7 M. However, a decrease in the corrosion potential is observed with further increase in the acid concentration to 9 M. Being an interstitial alloy, the protection to corrosion

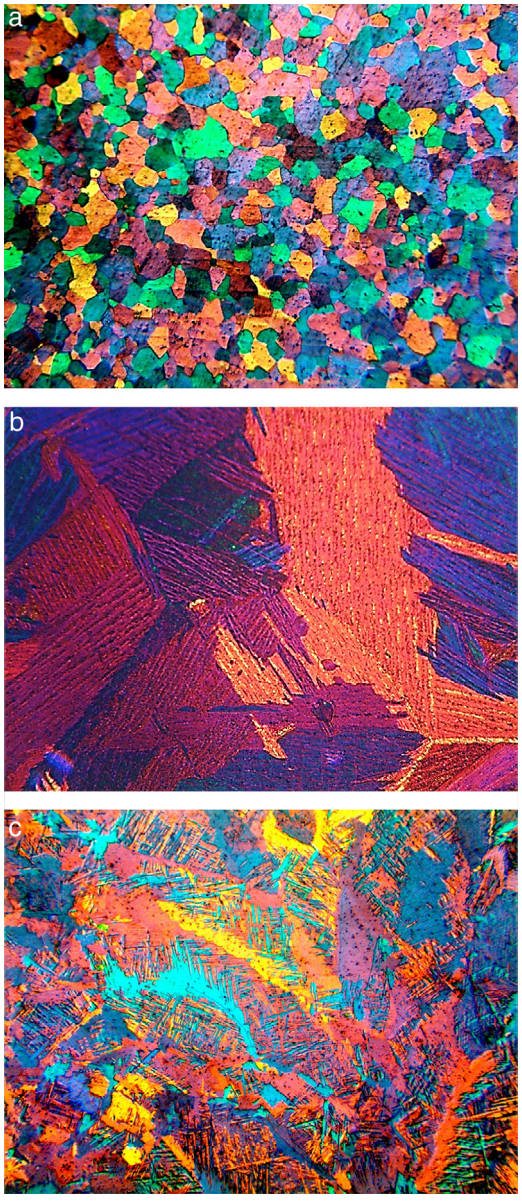

Fig. 5 – Microstructure of different zones (a) BM, (b) FZ of TIG welding and (c) FZ of laser welding.

Table 3 – Measurement of E_{corr} (V vs. Ag/AgCl) and I_{pass} (A/cm^2) of BM, TIG welded and laser welded Ti–5Al–2.5Sn.in different concentrations of HNO_3.

Nitric acid	E_{corr} (V vs. Ag/AgCl)	I_{pass} (μA/cm^2)
BM		
5 M HNO_3	$0.170 \pm 5.0 \times 10^{-4}$	$43.0 \pm 0.6.7$
7 M HNO_3	$0.270 \pm 5.0 \times 10^{-3}$	64.4 ± 1.92
9 M HNO_3	$0.190 \pm 3.4 \times 10^{-7}$	74.2 ± 2.44
TIG welded		
5 M HNO_3	$0.025 \pm 2.0 \times 10^{-3}$	46.0 ± 6.05
7 M HNO_3	$0.234 \pm 1.05 \times 10^{-2}$	66.3 ± 5.76
9 M HNO_3	$0.120 \pm 1.05 \times 10^{-2}$	67.7 ± 8.00
Laser welded		
5 M HNO_3	$0.063 \pm 1.05 \times 10^{-3}$	224 ± 3.00
7 M HNO_3	$0.161 \pm 1.05 \times 10^{-3}$	113 ± 7.30
9 M HNO_3	$0.140 \pm 9.0 \times 10^{-3}$	82.7 ± 3.75

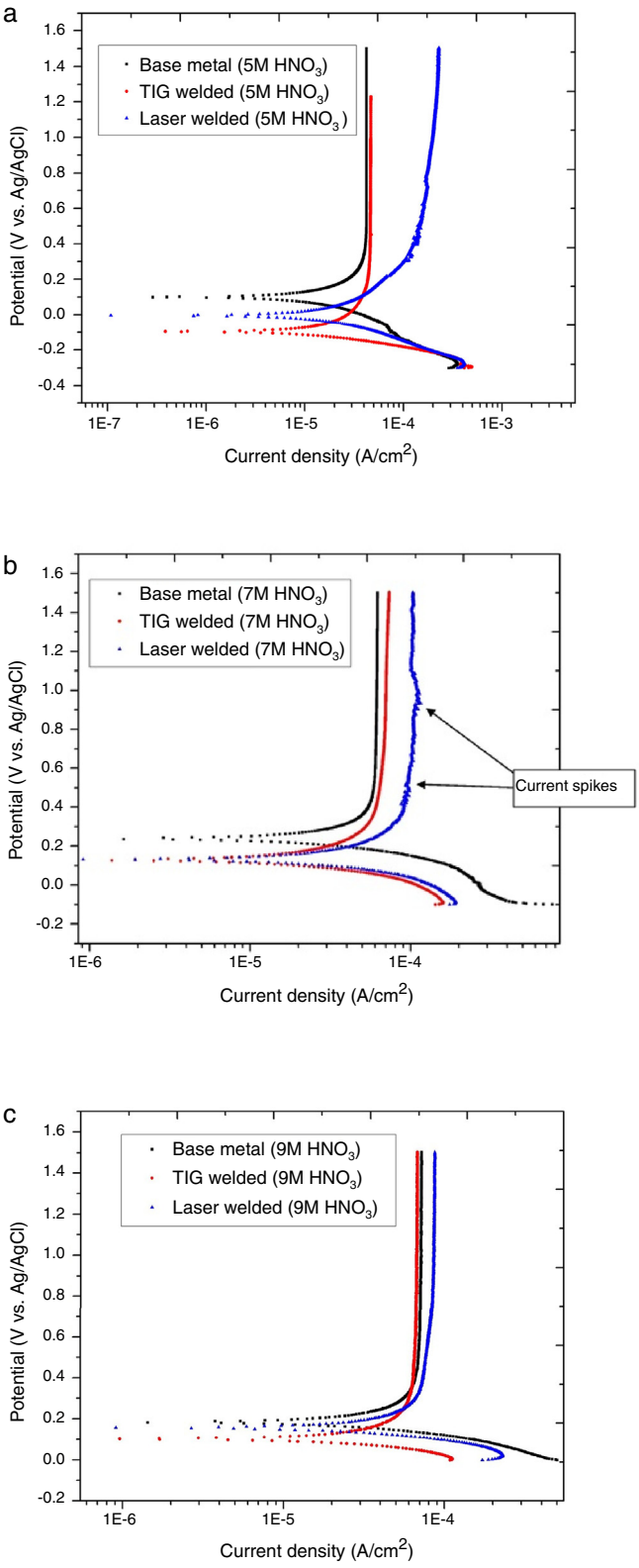

Fig. 6 – Potentiodynamic polarization curves for BM, TIG welded and laser welded Ti–5Al–2.5Sn in (a) 5 M HNO_3, (b) 7 M HNO_3 and (c) 9 M HNO_3.

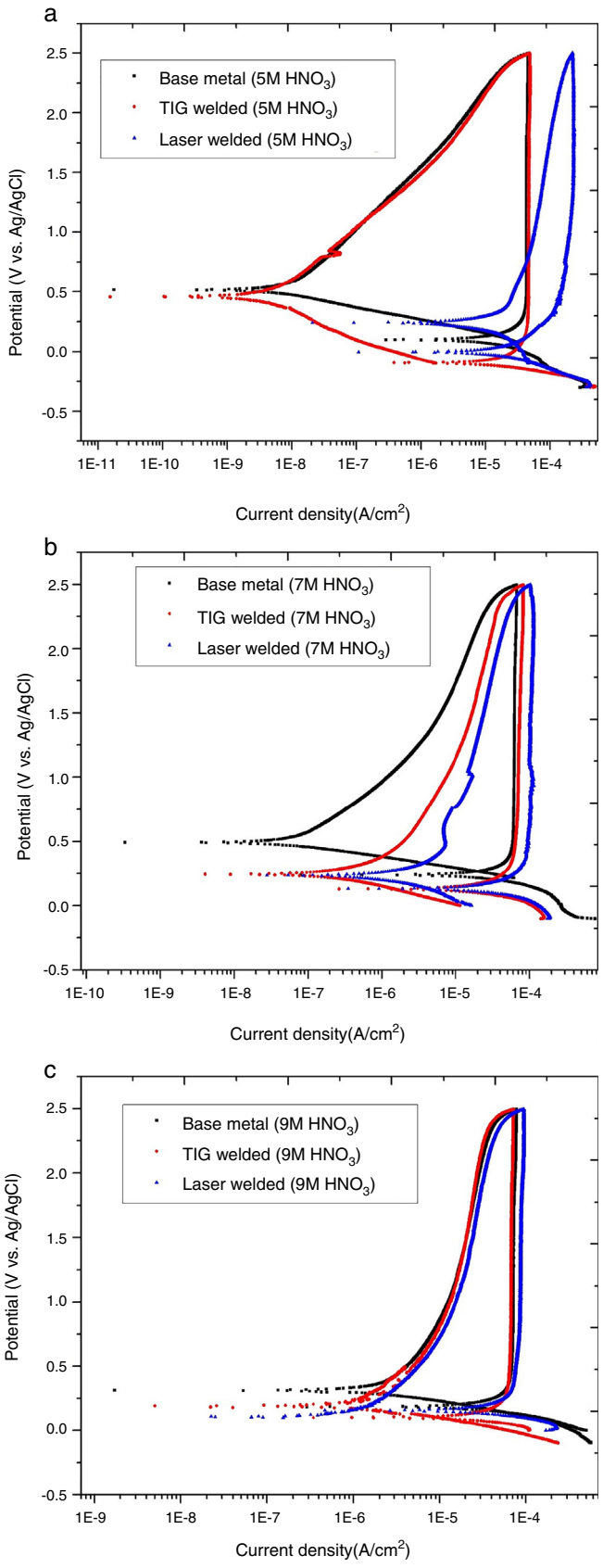

Fig. 7 – Cyclic polarization curves for BM, TIG welded and laser welded Ti–5Al–2.5Sn in (a) 5 M HNO_3, (b) 7 M HNO_3 and (c) 9 M HNO_3.

is mainly because of the titanium oxide layer. According to Pourbaix diagram, the potential range is on the boundary of Ti_2O_3 stable protection film formation and dissolution to TiO^{+2} [41,42]. When the concentration is increased from 5 to 7 M, the rate of reaction (oxidation) is higher compared to layer dissolution, thus resulting in thicker passive layer with increased resistance for the electron transfer at Fermi level and higher E_{corr} [30]. On the other hand, further decrease in pH results in higher solubility rates of oxide into the solution and decreases the corrosion potential. The same phenomenon can also be inferred from passivation current data. TIG welding generates Gaussian type heat affected zones of higher area compared to laser point welding, resulting in less passivation currents for TIG compared to laser welding (high temperature affected) counter parts. Furthermore, increasing acid concentration generally increases the passivation current (enhances layer solubility) as observed for BM and TIG specimen. Conversely, the opposite behavior exhibited by laser welding requires further insight for explanation.

Fig. 7 demonstrates the cyclic polarization curves of BM, TIG and laser welding. All these tests were performed in 5 M, 7 M and 9 M HNO_3. The loop areas of the cyclic polarization curves were measured using Gamry E-Chem Analyst and the loop areas are shown in Fig. 8. The reverse scan curve of all three concentrations came above the forward scan, which indicates that, the Ti–5Al–2.5Sn is resistant to pitting corrosion in different concentrations of HNO_3. The pitting corrosion resistance of any coating or material is ranked based on the loop area of the cyclic polarization curves. The higher the loop area, the poorer is the resistance to pitting corrosion and vice versa [1]. As it can be seen in Fig. 7 that the BM, TIG welded and laser welded Ti–5Al–2.5Sn forms a negative hysteresis loop for all the concentrations of HNO_3, suggesting that the BM does not undergo pitting corrosion. The areas of the loop, however, provide information about the pitting potential of this alloy in specific media. As the concentration increases from 5 M to 9 M, the loop area of BM deceases from $67.9 \times 10^{-3} \pm 4.05 \times 10^{-3}$ C/cm^2 to $45.3 \times 10^{-3} \pm 7.00 \times 10^{-3}$ C/cm^2. Similar trend was followed by the samples produced by TIG welding process. In case of TIG Ti–5Al–2.5Sn, the area of the loop decreases from $65.3 \times 10^{-3} \pm 1.36 \times 10^{-3}$ C/cm^2 to

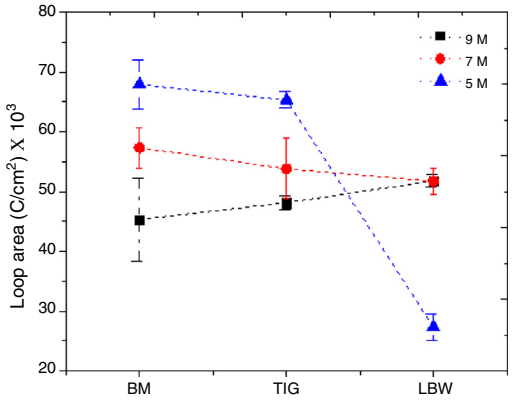

Fig. 8 – Loop areas calculated from cyclic polarization curves of BM, TIG welded and laser welded Ti–5Al–2.5Sn alloy in different concentration of HNO_3.

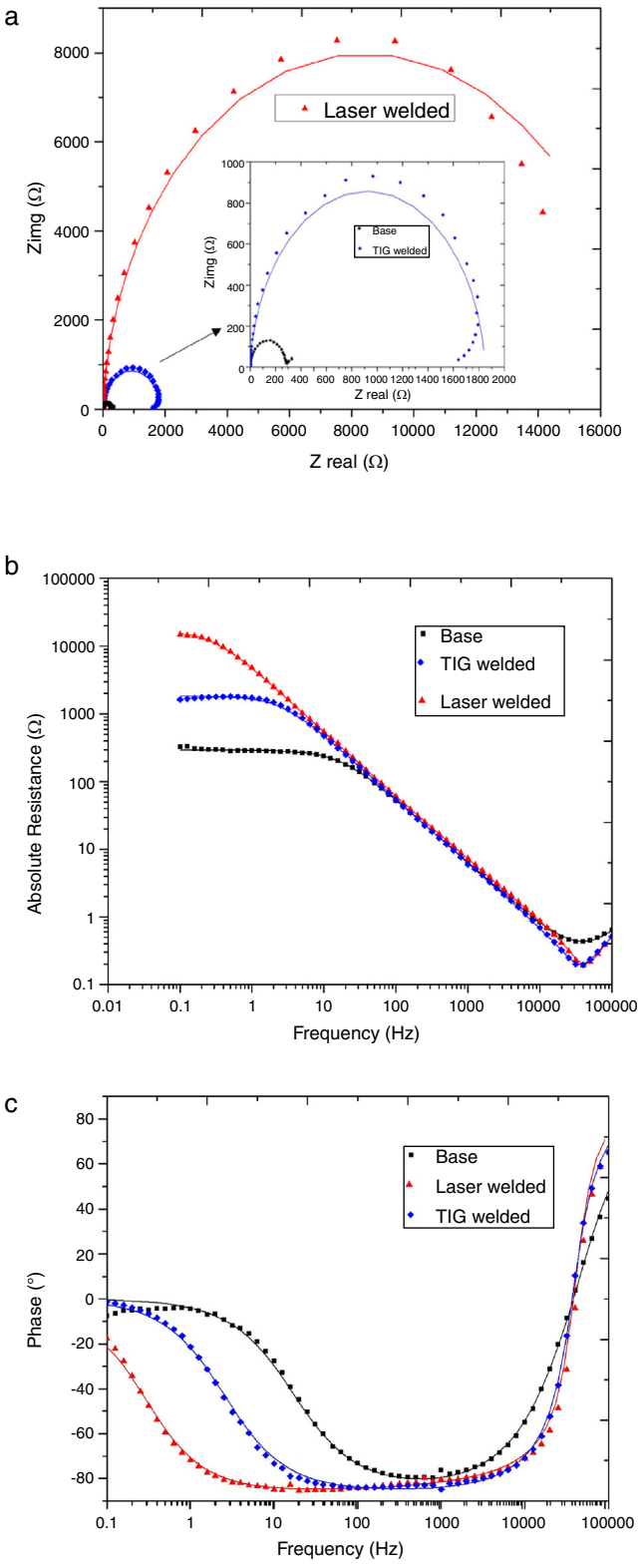

Fig. 9 – (a) Nyquist, (b) Bode resistance and (c) phase plots for the BM and welded Ti–5Al–2.5Sn after 192 h.

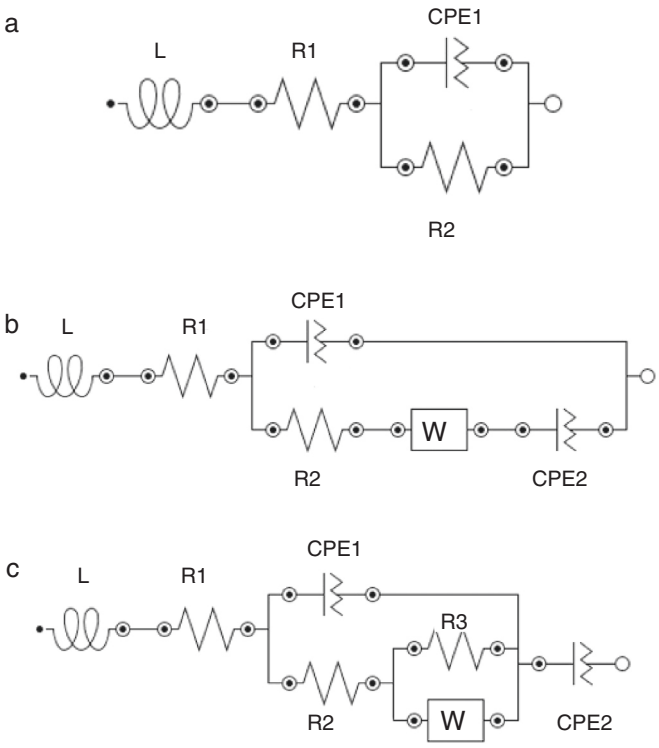

Fig. 10 – Schematic of equivalent circuit of (a) BM, (b) TIG and (c) laser welded Ti–5Al–2.5Sn after 192 h of immersion in 14.33 M HNO_3.

$48.1 \times 10^{-3} \pm 1.06 \times 10^{-3}$ C/cm^2, whereas, different trend was observed in case of laser welded Ti–5Al–2.5Sn. The areas of the loop increased from $27.3 \times 10^{-3} \pm 2.17 \times 10^{-3}$ C/cm^2 to $52.8 \times 10^{-3} \pm 1.12 \times 10^{-3}$ C/cm^2. The increase in the loop areas signifies the sample is less prone to pitting at higher concentrations. From the loop areas shown in Fig. 8, it can be seen that at 5 M HNO_3 BM has the highest loop area. The TIG welded Ti–5Al–2.5Sn area remains in the middle and laser welded Ti–5Al–2.5Sn has the least loop area. At 5 M HNO_3 laser welded Ti–5Al–2.5Sn is more resistant to pitting corrosion as compared to BM and TIG welded Ti–5Al–2.5Sn. At 7 M HNO_3 the difference between the loop areas of all three samples is almost negligible and the difference is reduced further at 9 M. Fig. 7 demonstrates that at 9 M HNO_3, the pitting potential of all the three samples is almost the same.

3.3. *Electrochemical impedance spectroscopy results*

EIS technique was employed in order to characterize the developed oxide layer on BM, TIG and laser welded samples. Fig. 9 shows the Nyquist, Bode resistance and phase plots for the BM and welded Ti–5Al–2.5Sn after 192 h of immersion in 14.33 M HNO_3. The solid lines in these figures show simulated plots, which were obtained by NOVA (AUTOLAB) model fitter, while the data points are from actual experimental results. Fig. 10 presents the equivalent circuits for the three samples and all the equivalent circuits show small inductance and resistance present because of the wires/connections and solution, respectively. Moreover, all the circuits show the double layer capacitance because of the presence of the passive layer. The

Table 4 – Value of resistances shown in Fig. 10.

Samples	L (μH)	R1 (mΩ)	R2 (kΩ)	R3 (kΩ)	CPE1 (μmho)	n1	CPE2 (mho)	n2	W (mho)
BM	1.41	712	0.45	–	30.7	0.945	–	–	–
TIG	1.10	203	1.49	–	30.6	0.949	110×10^{3}	1.00	1.10×10^{12}
Laser welded	0.93	145	12.5	2.34	38	0.96	1.56×10^{-3}	0.717	0.9×10^{-12}

upper parallel circuit constant phase element (CPE) conductance values of 30.7, 30.6 & 38 μMho for the BM, TIG and laser welded samples respectively (Table 4), confirms that the passive layer on the non/less-heat affected zone is intact. Furthermore, the values of '*n*' are close to '1' thus any major distortion in the surface layer is ruled out. The parallel circuit in the BM sample is simply a resistance of 448 Ω, typically representing an RC circuit for the passive layer having realistic values, with no pit formation. Warburg resistance, according to Sánchez et al. [43], should be present in the circuit when defects are introduced in the passive layer. TIG and laser welded sample show Warburg resistance; however, the former has only one time constant compared to two time constants for the later. The welding zone in nitric acid leads to the formation of two passive layers. The inner layer is intact compared to the outer layer, which develop pores, because of the metastable pitting. This outer layer for laser welded sample is not as corrugated as for TIG sample thus showing two time constants. This can also be inferred from the circuit elements positioning and values. The first resistance is 1.49 kΩ and 12.5 kΩ for the TIG and laser welded sample, showing smaller pores, resulting in higher resistance. The Warburg conductance of 1.10 TMho and 900 fMho for TIG and laser welded samples respectively, clearly leads to the same conclusion. Finally, for TIG, the last constant phase element is in series with the Warburg resistance, indicating that the second double layer is only present for the created pores. On the other hand, the same constant phase element, for laser welded sample, is in series to the parallel circuit of the first double layer and the Warburg resistance. This shows that the second passive layer, although porous, is still intact and provides some protection to the alloy surface from corrosion.

3.4. *Oxide layer analysis*

The SEM images (before and after acid treatment) of BM, laser welded and TIG welded Ti–5Al–2.5Sn are shown in Fig. 11. It can be inferred from the BM image that impurities in Ti–5Al–2.5Sn alloy precipitates preferably at the grain boundaries, whereas, the grain surface is homogeneous. This is because the melting point of the aluminum (660 °C) and tin (232 °C) is less than the titanium (1668 °C). When exposed to acid, the grain boundaries are consumed, as the impurity passive layer is not protective. Aluminum and tin usually form soluble salts with nitric acid and water and it is titanium, which provides the passivity to the alloy. This is the reason why pits start to develop at the boundaries, but do not propagate because of the presence of the titanium underneath. The homogenous grain does not show appreciable corrugation. The FZ of TIG leads to the formation of acicular grains because of rapid cooling. However, impurities emerge on the surface in high temperature zone and when treated with acid, these are washed away revealing actual grains. The small acicular grains leads to the formation of a stressed surface compared to the surface without weld. The combined effect of stress and impurity oxidation results in surface stress corrosion, leading to the formation of a porous passive layer. For laser welded samples, the heat-affected zone is relatively small, resulting in relatively smaller grains. However, these grains are less than the threshold size to introduce stress enhanced corrosion and thus introduce a second time constant in EIS. The high passive currents observed in Tafel plots for laser welded sample may be because of the relatively smaller grain size. As the grain boundaries results in impurity sensitization, thus exposing more subsurface area for passive current conduction.

4. Conclusions

After performing extensive corrosion tests on the BM, TIG and laser welded Ti–5Al–2.5Sn alloy sheets in 5, 7 and 9 HNO_3 following conclusions were drawn:

- The potentiodynamic polarization plots suggest the comparative kinetics of oxidation shifted to passive layer dissolution for BM and TIG samples. The high passive current for laser welding indicated that the exposed area to the acid was higher because of the grain boundaries sensitization, with subsequent dissolution of the formed oxides. This resulted in high surface area because of the exposed depths beneath the surface.
- Cyclic polarization scans did not confirm any stable pit formation since a negative hysteresis loop was observed in the cyclic polarization scan.
- EIS and equivalent circuit established the distinctive corrosion behavior for BM, TIG and laser welded samples. BM sample converged to simple RC circuit confirming good passivity in fuming HNO_3. TIG samples showed one time constant with Warburg resistance, confirming deterioration in the passive layer with local high concentration cells at the surface. However, these high concentration cells did not instigate visible pitting because of the better protection by titanium oxide. laser welded samples show two time constants, suggesting the formation of initial metastable pits and smaller concentration cells than in TIG sample.
- SEM images confirm sensitization to some degree in all the samples, i.e. BM, TIG and laser welded. The different grains sizes in the BM, TIG and laser welded samples, which were responsible for the unique EIS equivalent circuit for each sample.

Funding

The authors would like to thank Ghulam Ishaq Khan Institute for providing funding for this project.

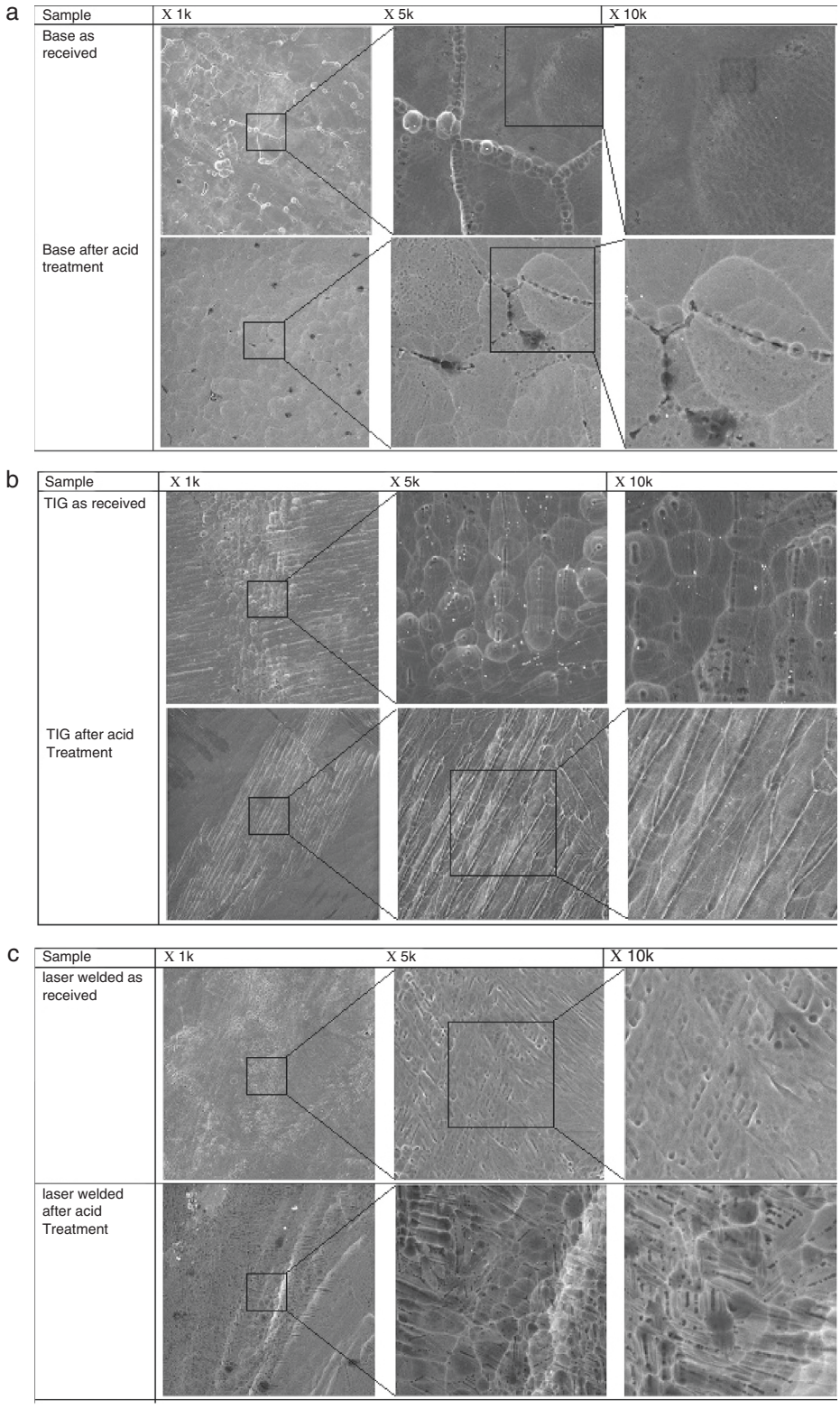

Fig. 11 – SEM images: (a) BM and acid treated BM, (b) TIG welded Ti–5Al–2.5Sn and after 192 h immersion in 14.33 M HNO_3 and (c) laser welded Ti–5Al–2.5Sn and after 192 h immersion in 14.33 M HNO_3.

Conflicts of interest

The authors declare no conflicts of interest.

Acknowledgments

The authors wish to thank Pakistan Welding Institute for use of research facilities.

REFERENCES

[1] Kumar S, Sankara Narayanan TSN. Electrochemical characterization of β-Ti alloy in Ringer's solution for implant application. J Alloys Compd 2009;479:699–703, http://dx.doi.org/10.1016/j.jallcom.2009.01.036.
[2] Choi BH, Choi BK. The effect of welding conditions according to mechanical properties of pure titanium. J Mater Process Technol 2008;201:526–30, http://dx.doi.org/10.1016/j.jmatprotec.2007.11.164.
[3] Akbari M, Saedodin S, Toghraie D, Shoja-Razavi R, Kowsari F. Experimental and numerical investigation of temperature distribution and melt pool geometry during pulsed laser welding of Ti6Al4V alloy. Opt Laser Technol 2014;59:52–9, http://dx.doi.org/10.1016/j.optlastec.2013.12.009.
[4] Rasouli S, Behnagh RA, Dadvand A, Saleki-Haselghoubi N. Improvement in corrosion resistance of 5083 aluminum alloy via friction stir processing. Proc Inst Mech Eng Part L J Mater Des Appl 2014:1–9, http://dx.doi.org/10.1177/1464420714552539.
[5] Yang X, Li S, Qi H. Ti–6Al–4V welded joints via electron beam welding: microstructure, fatigue properties, and fracture behavior. Mater Sci Eng A 2014;597:225–31, http://dx.doi.org/10.1016/j.msea.2013.12.089.
[6] Wu M, Xin R, Wang Y, Zhou Y, Wang K, Liu Q. Microstructure, texture and mechanical properties of commercial high-purity thick titanium plates jointed by electron beam welding. Mater Sci Eng A 2016;677:50–7, http://dx.doi.org/10.1016/j.msea.2016.09.030.
[7] Lu W, Li X, Lei Y, Shi Y. Study on the mechanical heterogeneity of electron beam welded thick TC4-DT joints. Mater Sci Eng A 2012;540:135–41, http://dx.doi.org/10.1016/j.msea.2012.01.117.
[8] Karpagaraj A, Siva N, Sankaranarayanasamy K. Some studies on mechanical properties and microstructural characterization of automated TIG welding of thin commercially pure titanium sheets. Mater Sci Eng A 2015;640:180–9, http://dx.doi.org/10.1016/j.msea.2015.05.056.
[9] Lathabai S, Jarvis BL, Barton KJ. Comparison of keyhole and conventional gas tungsten arc welds in commercially pure titanium. Mater Sci Eng A 2001;299:81–93, http://dx.doi.org/10.1016/S0921-5093(00)01408-8.
[10] Yunlian Q, Ju D, Quan H, Liying Z. Electron beam welding, laser beam welding and gas tungsten arc welding of titanium sheet. Mater Sci Eng A 2000;280:177–81, http://dx.doi.org/10.1016/S0921-5093(99)00662-0.
[11] Gao X-L, Zhang L-J, Liu J, Zhang J-X. A comparative study of pulsed Nd:YAG laser welding and TIG welding of thin Ti6Al4V titanium alloy plate. Mater Sci Eng A 2013;559:14–21, http://dx.doi.org/10.1016/j.msea.2012.06.016.
[12] Baldwin W. Metallography and microstructures 2004 ASM. Managing 2004;9:2733, http://dx.doi.org/10.1361/asmhba0003771.
[13] Calderon-Moreno JM, Vasilescu C, Drob SI, Ivanescu S, Osiceanu P, Drob P, et al. Microstructural and mechanical properties, surface and electrochemical characterisation of a new Ti–Zr–Nb alloy for implant applications. J Alloys Compd 2014;612:398–410, http://dx.doi.org/10.1016/j.jallcom.2014.05.159.
[14] Boyer RR. An overview on the use of titanium in the aerospace industry. Mater Sci Eng A 1996;213:103–14, http://dx.doi.org/10.1016/0921-5093(96)10233-1.
[15] Chamanfar A, Pasang T, Ventura A, Misiolek WZ. Mechanical properties and microstructure of laser welded Ti–6Al–2Sn–4Zr–2Mo (Ti6242) titanium alloy. Mater Sci Eng A 2016;663:213–24, http://dx.doi.org/10.1016/j.msea.2016.02.068.
[16] Hosseini S, Mirdamadi S, Nemati A. Porous Ti6Al4V scaffolds for dental implants: microstructure, mechanical, and corrosion behavior. Proc Inst Mech Eng L J Mater Des Appl 2015:1–7, http://dx.doi.org/10.1177/1464420715588218.
[17] Karimzadeh F, Heidarbeigy M, Saatchi A. Effect of heat treatment on corrosion behavior of Ti–6Al–4V alloy weldments. J Mater Process Technol 2008;206:388–94, http://dx.doi.org/10.1016/j.jmatprotec.2007.12.065.
[18] Madyira D, Laubscher R, van Rensburg NJ, Henning P. High speed machining induced residual stresses in Grade 5 titanium alloy. Proc Inst Mech Eng L J Mater Des Appl 2012;227:208–15, http://dx.doi.org/10.1177/1464420712462319.
[19] Barreda JL, Santamar FH, Azpiroz X, Irisarri AM, Varona JM. Electron beam welded high thickness Ti6Al4V plates using filler metal of similar and different composition to the base plate. Vacuum 2001;62:143–50.
[20] Baruah M, Bag S. Microstructural influence on mechanical properties in plasma microwelding of Ti6Al4V alloy. J Mater Eng Perform 2016;25:4718–28, http://dx.doi.org/10.1007/s11665-016-2333-8.
[21] Li X. Effects of oxygen contamination in the argon shielding gas in laser welding of commercially pure titanium thin sheet. J Mater Sci 2005:3437–43.
[22] Karpagaraj A, Siva shanmugam N, Sankaranarayanasamy K. Some studies on mechanical properties and microstructural characterization of automated TIG welding of thin commercially pure titanium sheets. Mater Sci Eng A 2015;640:180–9, http://dx.doi.org/10.1016/j.msea.2015.05.056.
[23] Junaid M, Nawaz F, Rahman K, Nadeem M. Effect of laser welding process on the microstructure, mechanical properties and residual stresses in Ti–5Al–2.5Sn alloy. Opt Laser Technol 2017, http://dx.doi.org/10.1016/j.optlastec.2017.07.010.
[24] Lu W, Shi Y, Lei Y, Li X. Effect of electron beam welding on the microstructures and mechanical properties of thick TC4-DT alloy. Mater Des 2012;34:509–15, http://dx.doi.org/10.1016/j.matdes.2011.09.004.
[25] Short AB. Gas tungsten arc welding of α + β titanium alloys: a review. Mater Sci Technol 2009;25:309–24, http://dx.doi.org/10.1179/174328408X389463.
[26] Vander Voort GF, Lampman SR, Sanders BR, Anton GJ, Polakowski C, Kinson J, et al. ASM handbook. Metallogr Microstruct 2004;9:44073–82.
[27] Mosleh A, Mahmoud F, Mahmoud T, Khalifa T. Microstructure and static immersion corrosion behavior of AA7020-O Al plates joined by friction stir welding. J Mater Des Appl 2015, http://dx.doi.org/10.1177/1464420715594484.
[28] Raj B, Mudali UK. Materials development and corrosion problems in nuclear fuel reprocessing plants. Progress Nucl Energy 2006;48:283–313, http://dx.doi.org/10.1016/j.pnucene.2005.07.001.
[29] Handbook M. Corrosion, vol. 13. ASM International; 1987. p. 584.
[30] Duarte LT, Biaggio SR, Rocha-Filho RC, Bocchi N. Surface characterization of oxides grown on the Ti–13Nb–13Zr alloy and their corrosion protection. Corros Sci 2013;72:35–40, http://dx.doi.org/10.1016/j.corsci.2013.02.007.

[31] Brytan Z, Niagaj J, Reiman L. Corrosion studies using potentiodynamic and EIS electrochemical techniques of welded lean duplex stainless steel UNS S82441. Appl Surf Sci 2016;388:160–8, http://dx.doi.org/10.1016/j.apsusc.2016.01.260.
[32] Liu J, Zhang L, Mu X, Zhang P. Studies of electrochemical corrosion of low alloy steel under epoxy coating exposed to natural seawater using the WBE and EIS techniques. Prog Org Coat 2017;111:315–21, http://dx.doi.org/10.1016/j.porgcoat.2017.06.012.
[33] ASTM. Standard guide for laboratory immersion corrosion testing of metals. ASTM International; 2012, http://dx.doi.org/10.1520/G0031-12A. G31–12a:1–10.
[34] Djokic S, Hansen D. Surface treatments for biomedical applications. Electrochem Soc 2008;11:1–12.
[35] Baruah M, Bag S. Influence of pulsation in thermo-mechanical analysis on laser micro-welding of Ti6Al4V alloy. Opt Laser Technol 2017;90:40–51, http://dx.doi.org/10.1016/j.optlastec.2016.11.006.
[36] Malinov S, Sha W, Guo Z, Tang C, Long A. Synchrotron X-ray diffraction study of the phase transformations in titanium alloys. Mater Charact 2002;48:279–95, http://dx.doi.org/10.1016/S1044-5803(02)00286-3.
[37] Pasang T, Sanchez Amaya JM, Tao Y, Amaya-Vazquez MR, Botana FJ, Sabol JC, et al. Comparison of Ti–5Al–5V-5Mo-3Cr welds performed by laser beam, electron beam and gas tungsten arc welding. Proc Eng 2013;63:397–404, http://dx.doi.org/10.1016/j.proeng.2013.08.202.
[38] Ahmed T, Rack HJ. Phase transformations during cooling in α + β titanium alloys. Mater Sci Eng A 1998;243:206–11, http://dx.doi.org/10.1016/S0921-5093(97)00802-2.
[39] Zeng L, Bieler TR. Effects of working, heat treatment, and aging on microstructural evolution and crystallographic texture of α, α′, α″ and β phases in Ti–6Al–4V wire. Mater Sci Eng A 2005;392:403–14, http://dx.doi.org/10.1016/j.msea.2004.09.072.
[40] Junaid M, Baig MN, Shamir M, Khan FN, Rehman K, Haider J. A comparative study of pulsed laser and pulsed TIG welding of Ti–5Al–2.5Sn titanium alloy sheet. J Mater Process Technol 2017;242:24–38.
[41] Heidarbeigy M, Karimzadeh F, Saatchi A. Corrosion and galvanic coupling of heat treated Ti–6Al–4V alloy weldment. Mater Lett 2008;62:1575–8, http://dx.doi.org/10.1016/j.matlet.2007.09.045.
[42] Balasubramanian M, Jayabalan V, Balasubramanian V. Modeling corrosion behavior of gas tungsten arc welded titanium alloy. Trans Nonferrous Met Soc China (Engl Ed) 2007;17:676–80, http://dx.doi.org/10.1016/S1003-6326(07)60155-1.
[43] Sánchez M, Gregori J, Alonso C, García-Jareño JJ, Takenouti H, Vicente F. Electrochemical impedance spectroscopy for studying passive layers on steel rebars immersed in alkaline solutions simulating concrete pores. Electrochim Acta 2007;52:7634–41, http://dx.doi.org/10.1016/j.electacta.2007.02.012.